The effects of junction interdiffusion and misfit dislocations on the efficiency of highly mismatched heterojunction photovoltaic devices

B.G. Mendis[1*], R.E. Treharne[2], D.W. Lane[3] and K. Durose[2]

1. *Dept. of Physics, Durham University, South Road, Durham, DH1 3LE, UK*
2. *Stephenson Institute for Renewable Energy, University of Liverpool, Chadwick Building, Liverpool, L69 7ZF, UK*
3. *Cranfield Forensic Institute, Cranfield University, Defence Academy of the United Kingdom, Shrivenham, SN6 8LA, UK*

Abstract

A general modelling methodology has been developed to evaluate the effects of chemical interdiffusion and misfit dislocations on the performance of heterojunction solar cells made from highly mismatched materials. Results for the exemplar materials system CdS-CdTe are contrary to the widely held belief that such interdiffusion is beneficial to photovoltaic performance. In the model, recombination is presumed to take place at the cores of misfit dislocations, with the distribution of these dislocations in the interdiffused layer being calculated so as to minimise the total energy (an incidental result shows that the total number of dislocations is independent of the diffusion profile). The model takes calculated chemical profiles, optical absorption and dislocation distributions from which the photovoltaic performance and recombination losses are evaluated. It was shown that for the realistic case in which the interdiffused region does not extend beyond the space charge region, then photovoltage losses dominate over any photocurrent gains. Methods to engineer mixed junctions that may increase solar conversion efficiency are discussed.

Manuscript

Arguably one of the last remaining challenges for thin film heterojunction photovoltaic (PV) devices is the deficit in open circuit voltage (V_{oc}) that they suffer in comparison to homo-junction or lattice matched heterojunctions. For example, while GaAs achieves a V_{oc} of ~80% of its band gap value, the present world record CdTe (21.0% conversion) is restricted to 876 mV, this being ~58% of band gap [1]. Should this shortfall be corrected then it is expected that CdTe PV devices will reach ~25% efficiency, i.e. comparable to the best wafer silicon. Accordingly there has been a resurgence of interest in single crystal CdTe devices and non-standard doping [2-3] in an attempt to realise higher V_{oc} performances than is achievable in polycrystalline thin films. However, for such highly mismatched systems the relative importance of misfit dislocations and of interdiffusion between the layers has not been estimated. Modelling the potential benefits of alloying and losses from recombination at (diffusion modified) misfit dislocations is the subject of this paper. The methodology is general and is developed for CdS-CdTe as an archetypal system. It has relevance to both epitaxial and polycrystalline devices.

Sulfur diffusion in CdS-CdTe photovoltaics forms a CdS_xTe_{1-x} layer at the interface [4-8] and is usually *assumed* to be beneficial [4,9] since it reduces the large (~10%) lattice mismatch

between CdS and CdTe. Electrical losses due to recombination are therefore presumed to be minimised. Furthermore, the variable band gap of CdS_xTe_{1-x} with respect to composition [10], raises the intriguing possibility of producing a graded band gap device. Graded gaps are utilised in $Cu(In,Ga)Se_2$ photovoltaics [11] and the $CdZn_xTe_{1-x}$ system has been proposed as an alternative to CdTe [12], the main advantage being the enhanced carrier collection due to the quasi-electric field [12]. A CdS_xTe_{1-x} graded band gap can be produced intentionally either by sputtering [13], isothermal close space sublimation [14] or unintentionally via the thermally induced diffusion from CdS into CdTe. In this letter numerical simulations of diffusion are carried out to determine its impact on photovoltaic device performance. The diffusion profile is calculated using diffusion coefficients for sulfur in bulk CdTe [15]. It has been shown that this satisfactorily reproduces the diffusion profile measured in real devices [8], so that the simulations are relevant to current device fabrication methodologies. Furthermore, a strain relaxation model is developed to calculate recombination losses at a chemically diffuse interface, which is applicable to other such structures as well. The findings challenge the accepted belief that CdTe-CdS interdiffusion can increase solar energy conversion efficiency in this device technology.

Figure 1 is a schematic of the device simulated and is based on the cell architecture fabricated in one of our labs (Liverpool). It consists of the glass superstrate (modelled as SiO_2; 3.2 mm thickness)/ F-doped SnO_2 transparent conducting oxide (TCO; 300 nm)/ ZnO barrier layer (100 nm)/ CdS (150 nm) and CdTe (5 µm). Complex refractive index values for CdTe are from [10] and the values for SiO_2, ZnO, SnO_2:F and CdS were obtained from ellipsometric measurements using a J.A. Woollam M2000 spectroscopic ellipsometer, with the SnO_2:F values being extracted from a sample of commercial TEC15 glass. Figure 2a is a band diagram for the CdS-CdTe interface under bias. The band shape and space charge width (W) within CdTe were calculated assuming the depletion approximation [16] and material parameters tabulated in the supplemental material [17]. For typical doping concentrations in CdS and CdTe (i.e. 10^{18} and 10^{15} cm^{-3} respectively) the space charge region and band bending is largely confined to the CdTe layer. In this particular example W has a value of 1.1 µm, which is consistent with experiment [23].

The photocurrent density at a given bias is due to photon absorption within the space charge region (SCR) as well as the minority carrier diffusion flux at the space charge edge [16]. For a given sulfur diffusion profile the former is calculated numerically using the absorption coefficient for CdS_xTe_{1-x} [10]. The current density due to diffusion is calculated from the steady-state minority carrier distribution (n) within the CdTe quasi-neutral region (QNR) [16]:

$$D_n \frac{\partial^2 n}{\partial z^2} + \frac{\alpha(z) I^{h\upsilon}(z)}{h\upsilon} - \frac{n}{\tau} = 0 \qquad \ldots (1)$$

The second term is the carrier generation profile due to absorption of light of energy $h\upsilon$ with absorption coefficient $\alpha(z)$. $I^{h\upsilon}(z)$ is the Air Mass 1.5 light energy flux [24] within the absorber layer after correcting for absorption and reflection from the preceding device layers. D_n is the minority carrier diffusion coefficient and τ is the lifetime; the values for bulk CdTe

(see supplemental material [17]) are used here since the sulfur diffusion profiles in this study do not extend significantly into the QNR. This also means that there is no drift term in Equation (1) due to the quasi-electric field of a graded band gap [12]. Equation (1) must be solved consistently with the boundary conditions at the space charge edge and CdTe back surface ([16]; see supplemental material [17]).

Modelling the strain distribution across the CdS_xTe_{1-x} layer is now discussed: figure 2b is a schematic of a chemically abrupt CdS-CdTe interface, where interfacial misfit dislocations are present to relieve the lattice mismatch. For this particular example the orientation relationship is CdS (0001) || CdTe (111) and CdS $[11\bar{2}0]$ || CdTe $[1\bar{1}0]$, so that for every ten CdTe atomic planes across the interface an extra half plane is present on the CdS side. Figure 2c is the equivalent diagram for a chemically diffuse interface drawn on a continuum scale. Because the mismatch is now spread out over the sulfur-diffusion distance, some of the misfit dislocations are swept further into the CdTe layer. The total energy (E) consists of the dislocation self energy (λ) and the strain energy due to lattice mismatch, the latter offset by the deformation (i.e. Burgers vector magnitude, b) required to create the dislocation [25]:

$$E = \lambda \int_0^{t_{CdTe}} \rho(z)dz + \mu_{el} \int_0^{t_{CdTe}} \left(\varepsilon(z) - b \int_0^z \rho(z')dz' \right)^2 dz \quad \ldots (2)$$

where μ_{el} is the elastic modulus and the mismatch parameter $\varepsilon(z) = [d(z)/d_{CdS}]$-1, with $d(z)$ being the local atomic planar spacing and d_{CdS} the value for bulk CdS. The dislocation density distribution $\rho(z)$ must minimise the energy E and is given by (see supplemental material [17]):

$$\rho(z) = \frac{1}{b}\left(\frac{d\varepsilon}{dz}\right) \quad \ldots (3)$$

It is assumed that relaxation takes place within the CdTe layer and not CdS, which is justified by the fact that the elastic moduli are larger for the latter [26]. The experimental lattice parameter values for CdS_xTe_{1-x} [21] are used to calculate $\rho(z)$ via Equation (3) for a given sulfur diffusion profile. Importantly it can be shown that the total number of dislocations is conserved and is independent of the sulfur diffusion profile (see supplemental material [17]). The physical reason for this is illustrated in Figures 2b and 2c. The Burgers circuit drawn across Figure 2b has no closure failure when transferred to a perfect bi-crystal and a similar principle applies to the chemically diffuse interface (Figure 2c). In each case the lattice mismatch between bulk CdS and CdTe is offset by the net dislocation strain field. The CdTe absorber layer in real devices is polycrystalline with a typically columnar structure [8, 23], so that the above situation is still applicable within the grain interiors, despite the presence of grain boundaries.

The recombination current density is calculated using the Shockley-Read-Hall (SRH) recombination rate (R) [16]:

$$R(z) = \frac{\sigma \upsilon_{\text{th}} N_t(z) n_i(z)^2 \left[\exp(qV/kT) - 1\right]}{\left[n(z) + p(z)\right] + \left[n_t(z) + p_t(z)\right]} \quad \ldots (4)$$

where q is the electronic charge, V the applied bias and kT has its usual meaning. σ is assumed here to be the 'geometric' capture cross-section valid for uncharged defect states (i.e. 10^{-15} cm^2; [16]), υ_{th} is the thermal velocity, (n,p) are the local electron, hole concentrations and $N_t(z)$ is the density of defect states at position z. Only atoms along the dislocation core are assumed to be SRH recombination centres, so that $N_t(z)$ can be calculated directly from $\rho(z)$. (n_t,p_t) are the electron, hole concentrations when the Fermi level is aligned with the defect energy level, which is taken to be in the middle of the local band gap. The final term in Equation (4) is the intrinsic carrier concentration (n_i), which is given by $n_i^2 = (N_c N_v)\exp(-E_g/kT)$, where N_c, N_v are the local density of states in the conduction and valence band respectively and E_g is the local band gap.

The recombination current density is determined by integrating Equation (4) over the space charge width W. It is useful to describe how the spatially varying parameters (e.g. $n_i(z)$, $n(z)$ etc) in Equation (4) are modified by sulfur diffusion. The permittivity, electron affinity and N_v for CdS_xTe_{1-x} are assumed to be identical to CdTe, since the values for bulk CdS and CdTe are similar (see supplemental material [17]). A constant permittivity means that the space charge width W and electrostatic potential are unchanged. The latter governs the shape of the vacuum energy level (E_{vac}; Figure 2a). The conduction band minimum is therefore also unchanged due to the constant electron affinity. The valence band maximum however does change due to a variable CdS_xTe_{1-x} band gap [10]. The quasi-Fermi levels within the SCR are as indicated in Figure 2a, which together with the band edge energies determine the local electron and hole concentrations (i.e. n, p, n_t and p_t; Equation (4)). The electron effective mass for CdS_xTe_{1-x} [19] is used to determine N_c. The variable band gap and N_c values mean that n_i in Equation (4) is a function of position.

525°C isothermal sulfur diffusion profiles were calculated for 'annealing' times of 10, 100, 200, 300, 400 and 500 mins, using experimental diffusion coefficients for sulfur in bulk CdTe [15]. 525°C/10 mins corresponds to the close space sublimation deposition conditions for CdTe in one of our labs (Liverpool). For these devices sulfur diffusion largely take place during absorber layer deposition, the 'thermal load' for post-deposition chlorine activation being comparatively smaller [8]. It is known from experiments [8] that for CdTe deposited at a higher temperature of 625°C for 60 mins, the increased sulfur diffusion consumes part of the CdS layer, so that these conditions represent an upper limit for practical device fabrication; indeed the most extreme condition of 525°C/500 mins in our simulations gives a diffusion profile similar to the experimental result for 625°C/60 mins. Representative sulfur diffusion profiles are shown in Figure 3 and indicate that the CdS_xTe_{1-x} layer does not extend beyond the ~1 μm wide SCR. For example a $CdS_{0.05}Te_{0.95}$ composition is obtained at 57, 181, 257, 314, 363 and 406 nm diffusion distance for 'annealing' times of 10, 100, 200, 300, 400 and 500 mins respectively.

Figure 4 shows simulated device parameter values as a function of 'annealing' time, in particular the short circuit current density (J_{sc}; Fig 4a), open circuit voltage (Fig 4b), fill factor (Fig 4c) and efficiency (Fig 4d). The efficiency decreases monotonically with sulfur diffusion, by as much as 3.4% after 500 mins. According to Equation (4) there is no recombination current at zero bias, so that the change in J_{sc} is due to photo-absorption within the CdS_xTe_{1-x} layer. However, Fig 4a indicates that this is a relatively small change, i.e. J_{sc} increases by only 0.6 mA/cm^2 after 500 mins. More appreciable changes are observed in the V_{oc} and fill factor, i.e. up to 87 mV and 8.2% decrease respectively, which suggests that the efficiency decrease is primarily due to recombination losses in CdS_xTe_{1-x}. The recombination current density (J_{rec}) at large positive bias (e.g. ≥ 0.2 V) can be approximated as:

$$J_{\text{rec}} = J_{r0} \exp\left(\frac{qV}{mkT}\right) \quad \text{... (5)}$$

where J_{r0} is a constant and m is the ideality factor. The latter has a maximum value of two for a defect level in the middle of the band gap and equal electron, hole concentrations throughout the SCR. On the other hand $m = 1$ for defects localised at a chemically abrupt CdS-CdTe interface (see supplemental material [17]). Figures 4e and 4f plot the J_{r0} and m-values as a function of 'annealing' time. There is a rapid increase in J_{r0} and the ideality factor approaches the maximum value with increased sulfur diffusion. This has the effect of reducing V_{oc} and fill factor (Figs 4b and 4c).

The increase in J_{r0} and m can be explained with the aid of the band diagram in Fig 2a. For no sulfur diffusion the misfit dislocations are localised at the CdS-CdTe interface, where the local electron concentration is significantly higher than the local hole concentration, leading to a relatively small SRH recombination rate. Sulfur diffusion does not reduce the total number of dislocations, but instead shifts the misfit dislocations further into the SCR where electron-hole concentrations are more equal and the SRH recombination rate is higher. The band diagram for a diffuse interface is somewhat different to Figure 2a, but the numerical results suggest that the overall trends are nevertheless still valid. The calculations also assumed a mid-gap defect energy level, although in practice it may vary during strain relaxation. Simulations were therefore also carried out with the defect energy set to shallower levels for the 525^{o}C/ 500 mins anneal, where sulfur diffusion, and hence strain relaxation, is greatest. Device efficiency showed very little improvement until the defect level had shifted by as much as 60% towards the conduction band edge (see supplemental material [17]). This degree of relaxation is however considered unlikely, particularly along the dislocations cores, where SRH recombination is assumed to occur in our model.

Thus unless the defect energy levels are shifted by more than 60% the conclusions in this letter, namely that sulfur diffusion is undesirable, holds true. It is worth mentioning however that there is hardly any change in efficiency for 10 mins 'annealing' time, which represents typical device fabrication conditions. For a sufficiently broad sulfur diffusion profile, such that some of the misfit dislocations are moved out of the SCR, the efficiency should start to increase due to decreasing recombination losses. Figure 3 shows that this cannot be practically achieved through natural diffusion from CdS, although there is still the possibility

of engineering a wider CdS_xTe_{1-x} layer through sputtering or isothermal close space sublimation. This could be explored experimentally.

In summary it has been shown that sulfur diffusion cannot improve device efficiency, despite minimising lattice mismatch at the CdS-CdTe interface. This is because the number of misfit dislocations is conserved, and sulfur diffusion shifts the dislocations further into the SCR, where the SRH recombination rate is higher. The effect is however predicted to be small for typical close space sublimated devices.

Acknowledgements

EPSRC funding for BGM (EP/I028781/1), KD (EP/J017361/1) and DWL (EP/F029624/2) is gratefully acknowledged. Raw data can be accessed at http://dx.doi.org/10.15128/xs55mc046.

Figure captions

Figure 1: Schematic of the simulated CdTe device with layer thicknesses indicated (figure not to scale).

Figure 2: (a) CdS-CdTe interface band diagram showing vacuum (E_{vac}), conduction band minimum (E_c) and valence band maximum (E_v) energy levels. χ, E_g are the electron affinity and band gap respectively. The electron and hole quasi-Fermi levels (E_{Fn} and E_{Fp}) are split due to the applied bias and are approximately equal to the Fermi level (E_F) within the respective bulk semiconductors. (b) and (c) are atomic and continuum-scale diagrams of the misfit dislocation distribution at a chemically abrupt and diffuse CdS-CdTe interface respectively. The CdS layer is at the bottom, while CdTe is on the top. The outer solid line represents the Burgers circuit.

Figure 3: Sulfur diffusion profiles at 525°C for 'annealing' times of 10, 200 and 500 mins.

Figure 4: Simulated values for (a) short circuit current density, (b) open circuit voltage, (c) fill factor, (d) efficiency, (e) J_{r0} and (f) ideality factor as a function of 'annealing' time at 525°C.

References

[1] M.A. Green, K. Emery, Y. Hishikawa, W. Warta, E.D. Dunlop, *Prog. Photovolt: Res. Appl.* (2015) **23**, 805.
[2] P.-Yu Su, C. Lee, G.-Ching Wang, T.-Ming Lu, I.B. Bhat, *J. Electron. Mater.* (2014) **43**, 2895.
[3] P.-Yu Su, R. Dahal, G.-Ching Wang, S. Zhang, T.-Ming Lu, I.B. Bhat, *J. Electron. Mater.* (2015) **44**, 3118.
[4] M. Terheggen, H. Heinrich, G. Kostorz, A. Romeo, D. Bätzner, A.N. Tiwari, A. Bosio, N. Romeo, *Thin Solid Films* (2003) **431-432**, 262.

[5] C. Li, N. Paudel, T.J. Pennycook, S.J. Haigh, M.M. Al-Jassim, Y. Yan, S.J. Pennycook, *IEEE Journal Photovoltaics* (2014) **4**, 1636.
[6] M. Emziane, K. Durose, N. Romeo, A. Bosio, D.P. Halliday, *Thin Solid Films* (2005) **480-481**, 377.
[7] U. Jahn, T. Okamoto, A. Yamada, M. Konagai, *J. Appl Phys* (2001) **90**, 2553.
[8] A.A. Taylor, J.D. Major, G. Kartopu, D. Lamb, J. Duenow, R.G. Dhere, X. Maeder, S.J.C. Irvine, K. Durose, B.G. Mendis, *Solar Energy Mat. Solar Cells* (2015) **141**, 341.
[9] H.C. Chou, A. Rohatgi, N.M. Jokerst, S. Kamra, S.R. Stock, S.L. Lowrie, R.K. Ahrenkiel, D.H. Levi, *Mat. Chem. Phys.* (1996) **43**, 178.
[10] D.A. Wood, K.D. Rogers, D.W. Lane, J.A. Coath, *J. Phys: Condens. Matter* (2000) **12**, 4433.
[11] R. Scheer, H.-W. Schock, *Chalcogenide Photovoltaics* (2011) Wiley-VCH, Germany.
[12] A. Morales-Acevedo, *Solar Energy Mat. Solar Cells* (2011) **95**, 2837.
[13] R.E. Treharne, B.L. Williams, L. Bowen, K. Durose, B.G. Mendis, (2012) Proc. 38th IEEE Photovoltaics Specialist Conference, Texas, pp. 001983-001987.
[14] O. de Melo, A. Domínguez, K. Gutiérrez Z-B, G. Contreras-Puente, S. Gallardo-Hernández, A. Escobosa, J.C. González, R. Paniago, J. Ferraz Dias, M. Behar, *Solar Energy Mat. Solar Cells* (2015) **138**, 17.
[15] D.W. Lane, G.J. Conibeer, D.A. Wood, K.D. Rogers, P. Capper, S. Romani, S. Hearne, *J. Cryst. Growth* (1999) **197**, 743.
[16] H.J. Möller, *Semiconductors for Solar Cells* (1993) Artech House, Boston, USA.
[17] Supplemental Material, which contains Refs. [12, 14-18], for further details on the simulation method, derivations on the dislocation density distribution, ideality factor and variable defect energy level.
[18] M. Gloeckler, A.L. Fahrenbruch, J.R. Sites (2003) Proc. 3rd World Conference PVSEC, Osaka, Japan, pp.491-494.
[19] D. Bhattacharyya, R. Pal, S. Chaudhuri, A.K. Pal, *Vacuum* (1993) **44**, 803.
[20] J. Ma, D. Kuciauskas, D. Albin, R. Bhattacharyya, M. Reese, T. Barnes, J.V. Li, T. Gessert, S-H. Wei, *Phys Rev Lett* (2013) **111**, 067402.
[21] D.A. Wood, K.D. Rogers, D.W. Lane, G.J. Conibeer, D. Parton, *J. Mat. Sci. Lett.* (1998) **17**, 1511.
[22] T. Dass, S.K. Sharma, *Mathematical Methods in Classical and Quantum Physics* (1998) University Press (India) Ltd, India.
[23] J.D. Major, L. Bowen, R. Treharne, K. Durose, *Prog. Photovolt: Res. Appl.* (2014) **22**, 1096.
[24] NREL Renewable Resource Data Centre (http://rredc.nrel.gov/solar/spectra/am1.5).
[25] J. Tersoff, *Appl. Phys. Lett.* (1993) **62**, 693.
[26] E. Deligoz, K. Colakoglu, Y. Ciftci, *Physica B* (2006) **373**, 124.

Figures

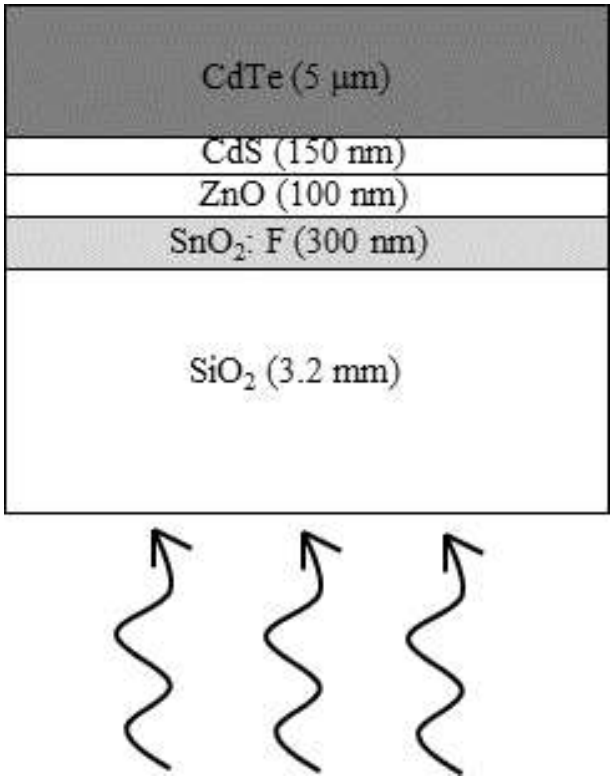

Figure 1

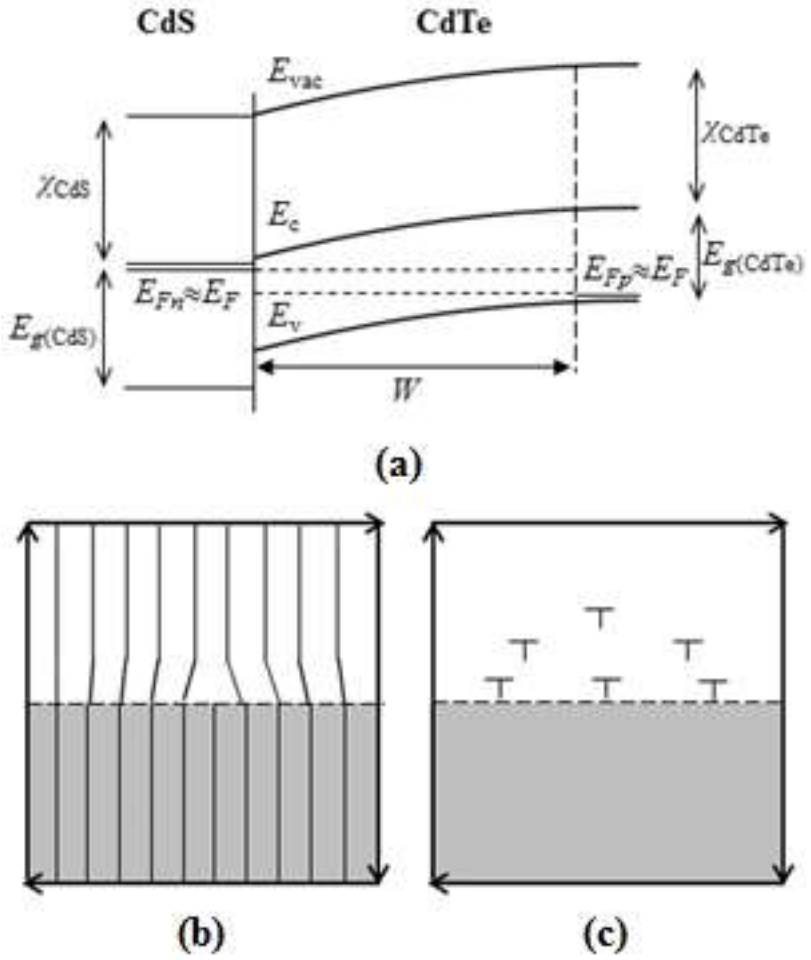

Figure 2

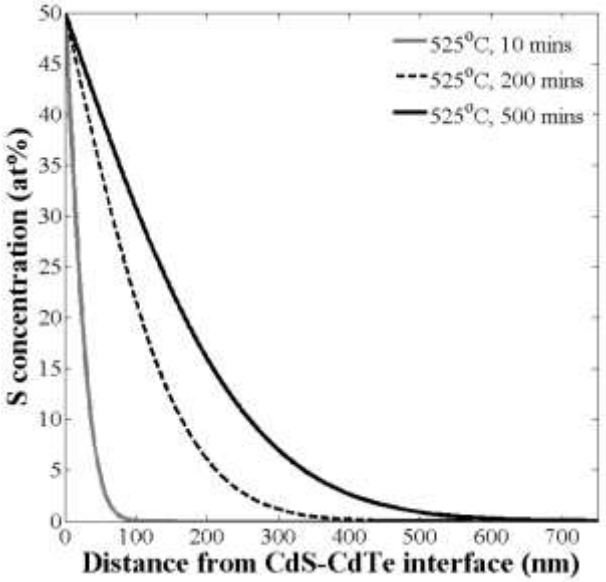

Figure 3

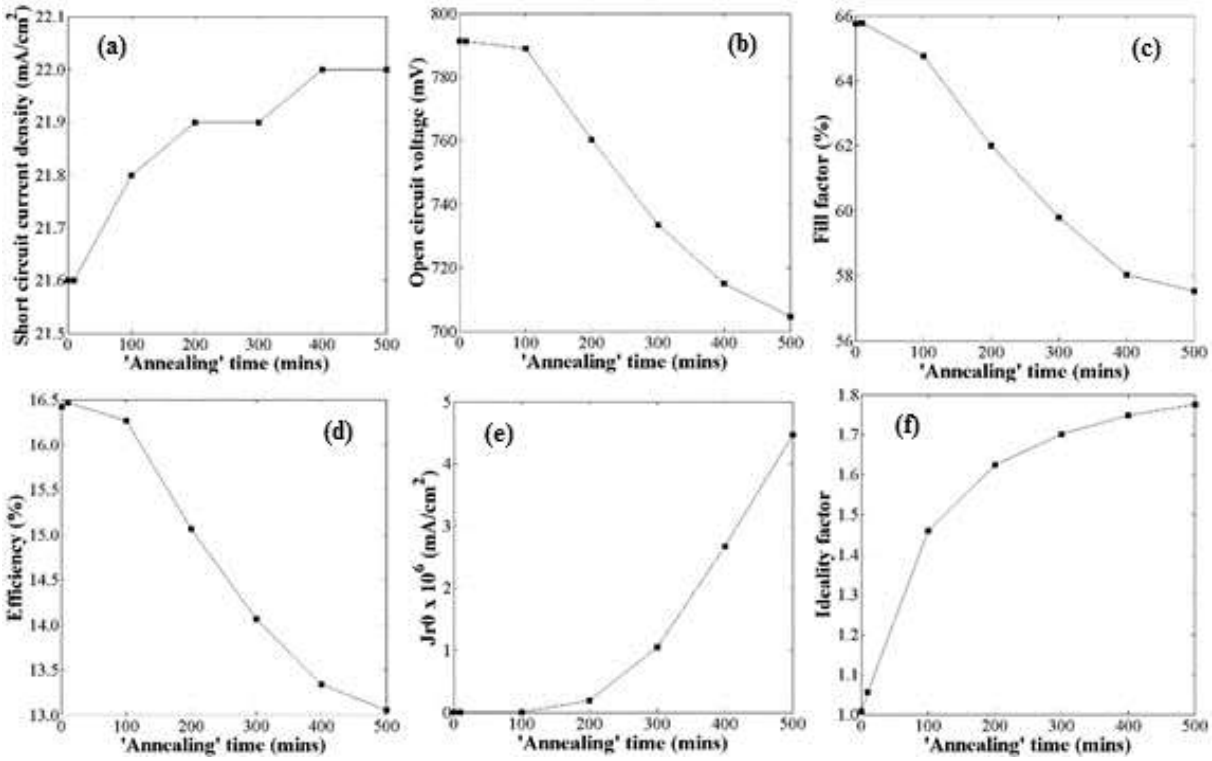
(a)
Short circuit current density (mA/cm^2)
'Annealing' time (mins)
(b)
Open circuit voltage (mV)
'Annealing' time (mins)
(c)
Fill factor (%)
'Annealing' time (mins)
(d)
Efficiency (%)
'Annealing' time (mins)
(e)
Jr0 x 10^{-6} (mA/cm^2)
'Annealing' time (mins)
(f)
Ideality factor
'Annealing' time (mins)

Figure 4